

We are IntechOpen, the world's leading publisher of Open Access books Built by scientists, for scientists

6,900

Open access books available

186,000

International authors and editors

200M

Downloads

Our authors are among the

154

Countries delivered to

TOP 1%

most cited scientists

12.2%

Contributors from top 500 universities



WEB OF SCIENCE™

Selection of our books indexed in the Book Citation Index
in Web of Science™ Core Collection (BKCI)

Interested in publishing with us?
Contact book.department@intechopen.com

Numbers displayed above are based on latest data collected.
For more information visit www.intechopen.com



Stability Analysis of Long Combination Vehicles Using Davies Method

*Gonzalo Guillermo Moreno Contreras,
Rodrigo de Souza Vieira and Daniel Martins*

Abstract

The cargo transportation in the world is mostly dominated by road transport, using long combination vehicles (*LCV*'s). These vehicles offer more load capacity, which reduces transport costs and thus increases the efficiency and competitiveness of companies and the country. But the tradeoff of *LCV*'s is their low lateral stability and propensity to roll over, which has been the focus of many studies. Most vehicle stability models do not consider the longitudinal aspects of the vehicle and the road, such as the stiffness of the chassis, the gravity center location, and the longitudinal slope angle of the road. But, the use of three-dimensional models of vehicles allows a more rigorous analysis of vehicle stability. In this context, this study aims to develop a three-dimensional mechanism model representing the last trailer unit of an *LCV* under an increasing lateral load until it reaches the rollover threshold. The proposed model considers the gravity center movement of the trailer, which is affected by the suspension, tires, fifth-wheel, and the chassis. Davies method has proved to be an important tool in the kinetostatic analysis of mechanisms, and therefore it is employed for the kinetostatic analysis of the three-dimensional mechanism of the trailer.

Keywords: stability, road safety, static rollover threshold (SRT)

1. Vehicle model for lateral stability

According to Rempel [1] and Melo [2], the last unit (semi-trailer) of an *LCV* is the critical unit, since it is subjected to a high lateral acceleration compared to the tractor unit, which impacts the rollover threshold of the unit and the vehicle. Taking into account this aspect, a simplified trailer model (**Figure 1**) is modelled and analysed to calculate the *SRT* factor for *LVC*s.

The tyres, suspension, fifth wheel, and chassis are directly responsible for the *CG* movements; these movements are dependent on the forces acting on the trailer *CG*, such as weight (W), disturbance forces imposed by the ground, and lateral inertial force (ma_y) when the vehicle makes a turn. During cornering or evasive manoeuvres, the weight and the lateral inertial force acting on the vehicle centre of gravity cause its displacement, which can lead to vehicle rollover.

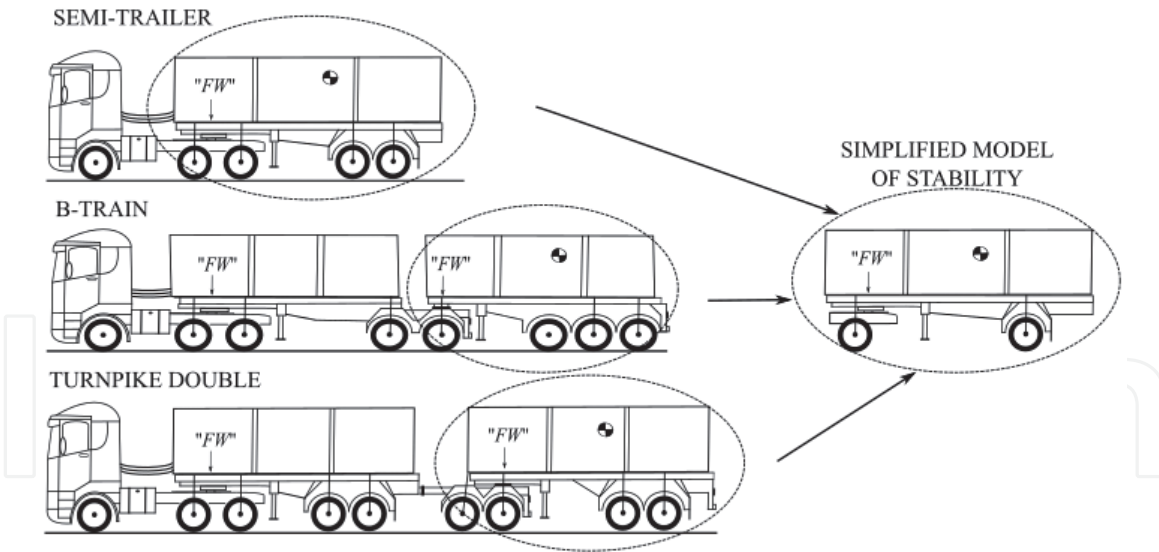


Figure 1.
Simplified trailer model.

1.1 Tyres system

The tyres system (tyres and rigid suspension) maintains contact with the ground and filters the disturbances imposed by road imperfections [3]. This system allows two motions of the vehicle: displacement in the z -direction and a roll rotation around the x -axis [4], as shown in **Figure 2**.

1.1.1 Kinematic chain for tyres system

Mechanical systems can be represented by kinematic chains composed of links and joints, which facilitate their modelling and analysis [5–7].

The kinematic chain of the tyres system in **Figure 2** has 2-DoF ($M = 2$), the workspace is planar ($\lambda = 3$), and the number of independent loops is one ($\nu = 1$). Based on the mobility equation, the kinematic chain of tyres system should be composed of five links ($n = 5$) and five joints ($j = 5$) [7].

To model this system, the following considerations were taken into account:

- There are up to three different components of forces acting on the tyre-ground contact i of the vehicle [8–10], as shown in **Figure 3**, where F_{xi} is the traction or brake force, F_{yi} is the lateral force, and F_{zi} is the normal force;
- However, at rollover threshold, tyres 1 and 4 (outer tyres in the turn, **Figure 4**) receive greater normal force than tyres 2 and 3 (inner tyre in the turn, **Figure 4**), and thus tyres 1 and 4 are not prone to slide laterally. We consider that tyres 1 and 4 only allow vehicle rotation along the x -axis. Therefore, tyre-ground contact was modelled as a pure revolute joint R along x -axis.

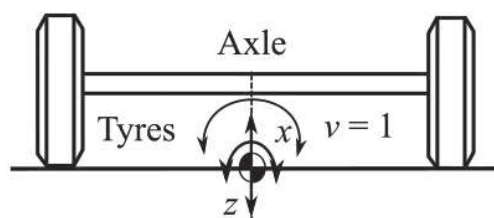


Figure 2.
Tyres system.

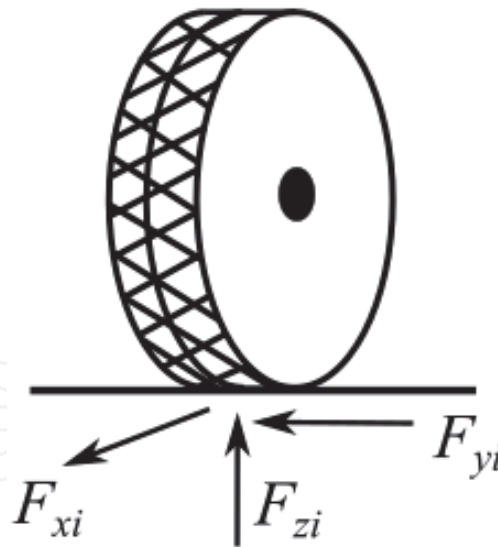


Figure 3.
 Movement constraints in Tyre-road contact.

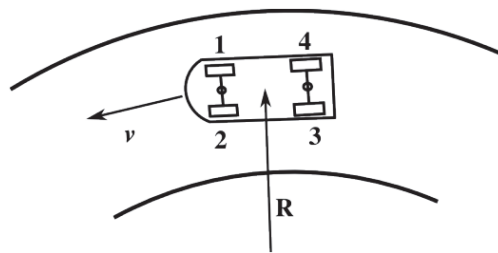


Figure 4.
 Vehicle on a curved path.

- While tyres 2 and 3 have a lateral deformation and may slide laterally, producing a track width change of their respective axles. As a consequence, tyres 2 and 3 have only a constraint on the z -direction. Therefore, tyre-ground contact was modelled as a prismatic joint P in the y -direction.
- Tyres are assumed as flexible mechanical components and can be represented by prismatic joints P , [11, 12].
- In vehicles with rigid suspension, tyres remain perpendicular to the axle all the time.

Applying these constraints, **Figure 5a** shows the proposed kinematic chain model of the tyres system.

The kinematic chain is composed of five links identified by letters A (road), B (outer tyre in the turn), C and D (inner tyre in the turn), and E (vehicle axle); and the five joints are identified by numbers as follows: two revolute joints R (tyre-road

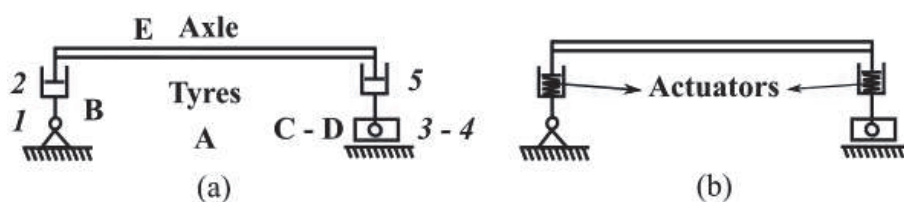


Figure 5.
 (a) Kinematic chain of the tyres system. (b) Tyres system including actuators.

contact of joints 1 and 4) and three prismatic joints P , two that represent tyres of the system (2 and 5), and one the lateral slide of tyre 2 (3).

The mechanism of **Figure 5a** has 2-DoF, and it requires two actuators to control its movement. The mechanism has a passive actuator in each prismatic joint of tyres (2 and 5—axial deformation); these actuators control the movement along the x - and z -axes, as shown in **Figure 5b**.

In this model, the revolute joint (3) and the prismatic joint (4) can be changed by a spherical slider joint (S_d), with constraint in the z -axis, as shown in **Figure 6**.

1.1.2 Kinematics of tyre system

The movement of this system is orientated by the forces acting on the mechanism (trailer weight (W) and the inertial force (ma_y)) [13]. These forces affect the passive actuators of the mechanism, as shown in **Figure 7**.

Eqs. (1)–(5) define the kinematics of the tyres system.

$$l_i = \delta_T + l_r = \frac{3\Delta F}{k_t + a_c} + l_r \approx \frac{-F_{Ti} + F_{zi}^{start}}{k_T} + l_r \quad (1)$$

$$\beta_i = 90 - \arcsin \left(\frac{l_{i+1}}{\sqrt{t_{i+1}^2 + l_{i+1}^2}} \right) \quad (2)$$

$$t_i = \sqrt{t_{i+1}^2 + l_{i+1}^2 + l_i^2 - 2 \left(\sqrt{t_{i+1}^2 + l_{i+1}^2} \right) l_i \cos(\beta_i)} \quad (3)$$

$$\delta_i = \arcsin(l_i \sin(\beta_i)/t_i) \quad (4)$$

$$\theta_i = \theta_j = 90 - \delta_i - \beta_i \quad (5)$$

where δ_T is the normal deformation of the tyre [14], ΔF is the algebraic change in the initial load, k_i is the vertical stiffness of the tyre, a_c is the regression coefficient, F_{Ti} is the instantaneous tyre normal load, l_i is the instantaneous dynamic rolling radius of the tyre i , F_{zi}^{start} is the initial normal load i , k_T is the equivalent tyre vertical stiffness, l_r is the initial dynamic rolling radius of tyre i , t_i is the track width,

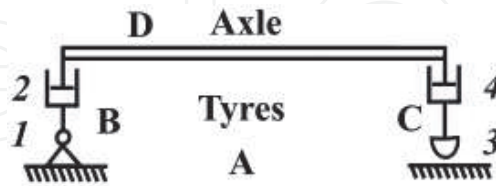


Figure 6.
Tyres system model.

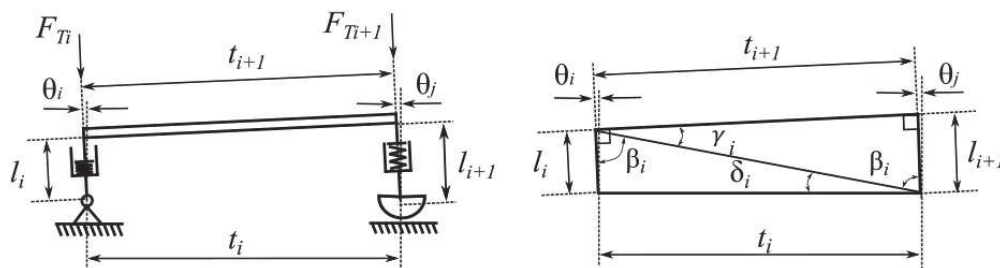


Figure 7.
Movement of tyres system.

t_{i+1} is the axle width, and $\theta_{i;j}$ are the rotation angles of the revolute joints i and j respectively.

1.2 Suspension system

This system comprises the linkage between the sprung and unsprung masses of a vehicle, which reduces the movement of the sprung mass, allowing tyres to maintain contact with the ground, and filtering disturbances imposed by the ground [3]. In heavy vehicles, the suspension system most used is the leaf spring suspension or rigid suspension [15], as shown in **Figure 8**. For developing this model (trailer), it is assumed that the vehicle has this suspension on the front and rear axles.

The rigid suspension is a mechanism that allows the following movements of the vehicle's body under the action of lateral forces: displacement in the z - and y -direction and a roll rotation about the x -axis [1, 8], as shown in **Figure 9a** and **b**.

1.2.1 Kinematic chain of the suspension system

The system of **Figure 10a** has 3-DoF ($M = 3$), the workspace is planar ($\lambda = 3$) and the number of independent loops is one ($\nu = 1$). From the mobility equation, the kinematic chain of suspension system should be composed of six links ($n = 6$) and six joints ($j = 6$).

To model this system the following consideration is considered: leaf springs are assumed as flexible mechanical components with an axial deformation and a small shear deformation, and can be represented by prismatic joints P supported in revolute joints R [16].

To allow the rotation of the body in the z -axis, the link between the body and the leaf spring is made with revolute joint. Applying these concepts to the system, a model with the configuration shown in **Figure 10b** is proposed.

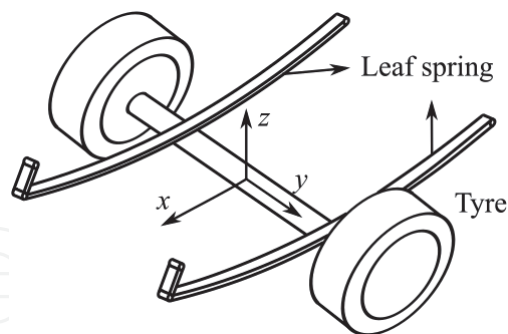


Figure 8. Solid axle with leaf spring suspension. Source: Adapted from Rill et al. [15].

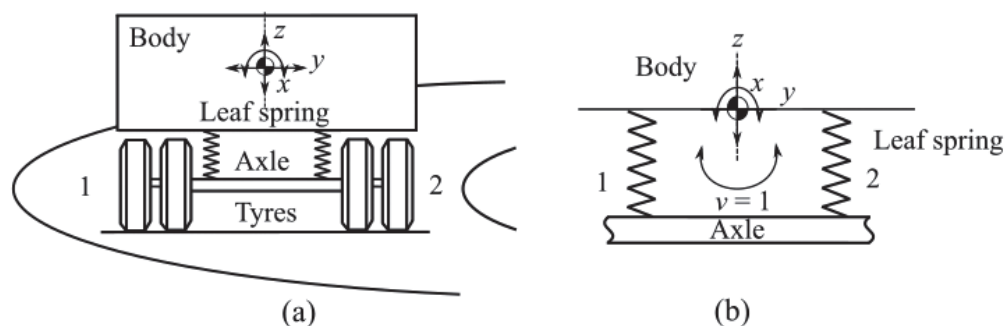
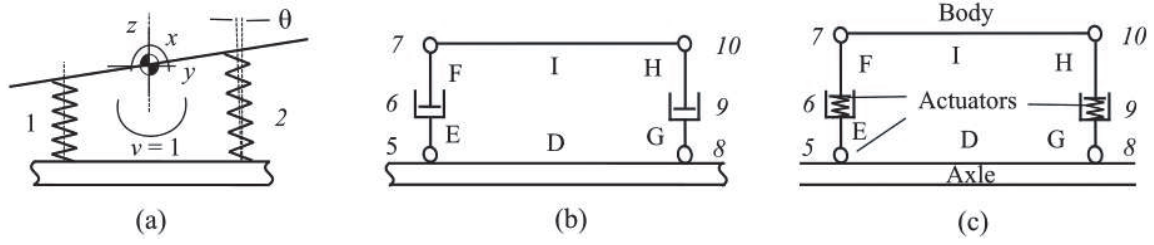


Figure 9. (a) Body motion. (b) Suspension system.


Figure 10.

(a) Movement of suspension system. (b) Kinematic chain of suspension system. (c) Suspension system including actuators.

The system is composed of six links identified by letters D (vehicle axle), E and F (spring 1), G and H (spring 2), and I (the vehicle body), and the six joints identified by the following numbers: four revolute joints R (5, 7, 8, and 10) and two prismatic joints P that represent the leaf springs of the system (6 and 9), as shown in **Figure 10b**.

The mechanism of **Figure 10b** has 3-DoF, and it requires three actuators to control its movements, applying the technique developed in Section 1.1, the kinematic chain has a passive actuator in the prismatic joints 6 and 9 (axial deformation of the leaf spring), and a passive actuator in the joints 6 and 9 (torsion spring—shear deformation); but the mechanism with four passive actuators is over-constrained, in this case only one equivalent passive actuator is used in the joint 5 or 8, as shown in **Figure 10c**.

1.2.2 Kinematics of the suspension system

The movement of the suspension is orientated first by the movement of the tyres system, and second by forces acting on the mechanism (vehicle weight (W) and inertial force (ma_y)). These forces affect the passive actuators of the mechanism, as shown in **Figure 11**.

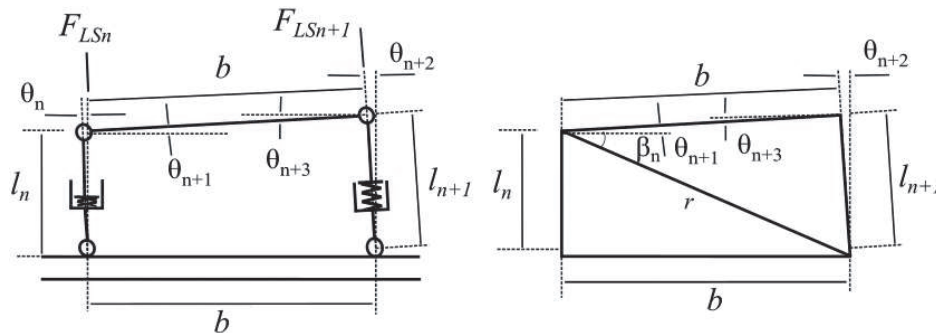
Eqs. (6)–(12) define the kinematics of the suspension system:

$$\theta_n = T_{xn}/k_{ts} \quad (6)$$

$$l_n = \delta_{LS} + l_s = \frac{3\Delta F l^3}{8E_s N B T^3} + l_s \approx \frac{-F_{LSn} + F_{zi}^{start}}{k_{LS}} + l_s \quad (7)$$

$$r = \sqrt{l_n^2 + b^2 - 2l_n b \cos(90 + \theta_6)} \quad (8)$$

$$\beta_n = \arccos((b^2 + r^2 - l_n^2)/(2br)) \quad (9)$$


Figure 11.

Movement of suspension system.

$$\theta_{n+1} = \beta_n + \arcsin \left(\frac{b}{r} \sin (90 + \theta_n) \right) - 90 \quad (10)$$

$$\theta_{n+2} = \theta_n + \arcsin \left(\frac{b}{r} \sin (90 + \theta_n) \right) - \arcsin \left(\frac{b}{l_{n+1}} \sin (\beta_n) \right) \quad (11)$$

$$\theta_{n+3} = 90 - \beta_n - \arcsin \left(\frac{b}{l_{n+1}} \sin (\beta_n) \right) \quad (12)$$

where T_{xn} is the moment around the x -axis on the joint n , k_{ts} is the spring's torsion coefficient, δ_{LS} is the leaf spring deformation [17], ΔF is the algebraic change in the initial load, l is the length of the leaf spring, N is the number of leaves, B is the width of the leaf, T is the thickness of the leaf, E_s is the modulus of elasticity of a multiple leaf, l_n is the instantaneous height of the leaf spring n , F_{LSn} is the spring normal force n , l_s is the initial suspension height, k_{L_s} is the equivalent stiffness of the suspension, l_n is the instantaneous height of the leaf spring n , b is the lateral separation between the springs, and θ_n is the rotation angle of the revolute joint n .

1.3 The fifth wheel system

This system is a coupling device between the tractive unit and the trailer; but in the case of a multiple trailer train, a fifth wheel also can be located on a lead trailer. The fifth wheel allows articulation between the tractive and the towed units.

This system consists of a wheel-shaped deck plate usually designed to tilt or oscillate on mounting pins. The assembly is bolted to the frame of the tractive unit. A sector is cut away in the fifth wheel plate (sometimes called a throat), allowing a trailer kingpin to engage with locking jaws in the centre of the fifth wheel [18]. The trailer kingpin is mounted in the trailer upper coupler assembly. The upper coupler consists of the kingpin and the bolster plate.

When the vehicle makes different manoeuvres (starting to go uphill or downhill, and during cornering) [18], the fifth wheel allows the free movement of the trailer and more flexibility of the chassis, as shown in **Figures 12–14**.

Rotation about the longitudinal axis of up to 3° of movement between the tractor and trailer is permitted. On a standard fifth wheel, this occurs as a result of clearance between the fifth wheel to bracket fit, compression of the rubber bushes, and also the vertical movement between the kingpin and locks may allow some lift of the trailer to one side [18].

Consider the third movement of the trailer, the mechanism that represents the fifth wheel has similar design and movements to the suspension mechanism (**Figure 15**), it is located over the front suspension mechanism.

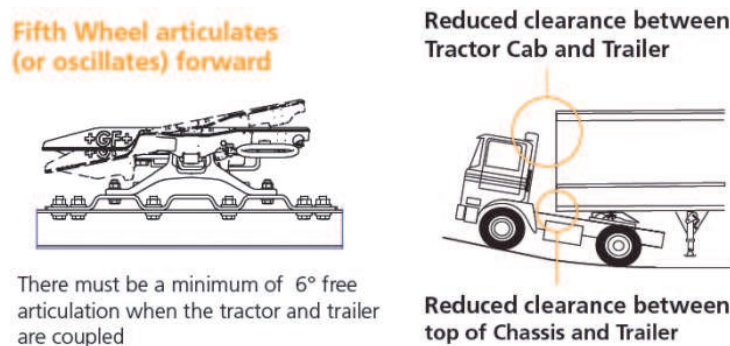
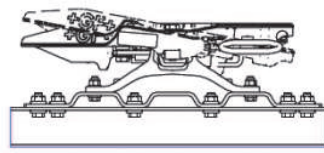
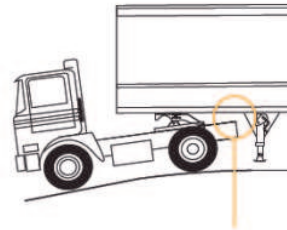


Figure 12. Movement of the fifth wheel—Starting uphill. Source: Adapted from Saf-Holland [18].

Fifth Wheel articulates (or oscillates) to the rear



There must be a minimum of 7° free articulation when the tractor and trailer are coupled



Reduced clearance between rear of Chassis and Trailer

Figure 13. Movement of the fifth wheel—Starting downhill. Source: Adapted from Saf-Holland [18].

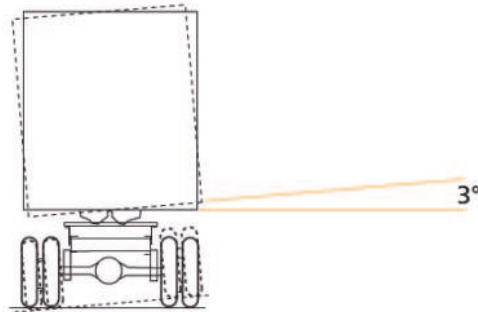


Figure 14. Movement of the fifth wheel—Rotation x-axis. Source: Adapted from Saf-Holland [18].

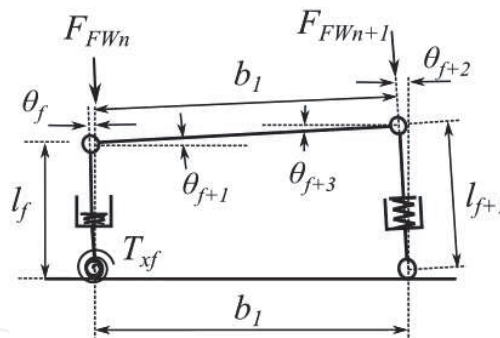


Figure 15. Kinematic chain of fifth wheel system.

Here l_{fw} is the fifth wheel system's instantaneous height, F_{FWn} is the fifth wheel normal load, and l_{fi} is the fifth wheel system's initial height, b_1 is the fifth wheel width.

1.4 The chassis

The chassis is the backbone of the trailer, and it integrates the main truck component systems such as the axles, suspension, power train, and cab. The chassis is also an important part that contributes to the dynamic performance of the whole vehicle. One of the truck's important dynamic properties is the torsional stiffness, which causes different lateral load transfers (LLT) on the axles of the vehicle [19].

According to Winkler [20] and Rill [4], the chassis has significant torsional compliance, which would allow its front and rear parts to roll independently; this is

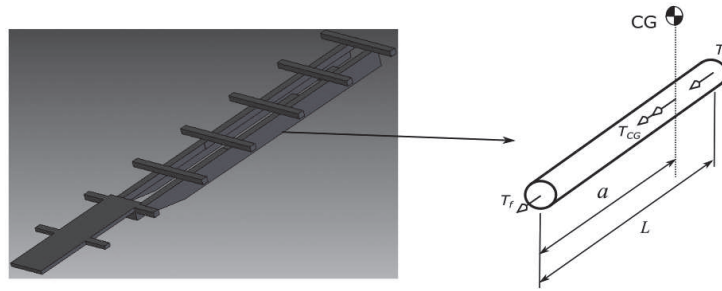


Figure 16.
 Kinematic chain of the chassis.

because the lateral load transfer is different on the axles of the vehicle. Then, applying the torsion theory, the vehicle frame has similar behaviour with a statically indeterminate torsional shaft, as shown in **Figure 16**.

Here T_{CG} is the torque applied by the forces acting on the CG, T_f (T_{28}) is the torque applied on the vehicle front axle, T_r (T_{27}) is the torque applied on the vehicle rear axle, a is the distance from the front axle to the centre of gravity, and L is the wheelbase of the trailer. Applying torsion theory to the statically indeterminate shaft, the next equation is defined:

$$\frac{T_f a}{J_f G} = \frac{T_r (L - a)}{J_r G} \quad (13)$$

where J_f and J_r are the equivalent polar moments on front and rear sections of the vehicle frame respectively, and G is the modulus of rigidity (or shear modulus).

According to Kamnik et al. [21] when a trailer model makes a spiral manoeuvre, the *LLT* on the rear axle is greater than the *LLT* on the front axle; therefore the equivalent polar moment on the rear (J_r) is greater than the equivalent polar moment on the front (J_f). These can be expressed as $J_r = x J_f$ (where x is the constant that allows controlling the torque distribution of the chassis); replacing and simplifying Eq. (13):

$$T_f + T_r \left(\frac{a - L}{ax} \right) = 0 \quad (14)$$

However, when the trailer model makes a turn, the torque applied on the vehicle front axle has two components, as shown in **Figure 17** and Eqs. (15) and (16).

$$T_{fx} = T_f \cos \psi \quad (15)$$

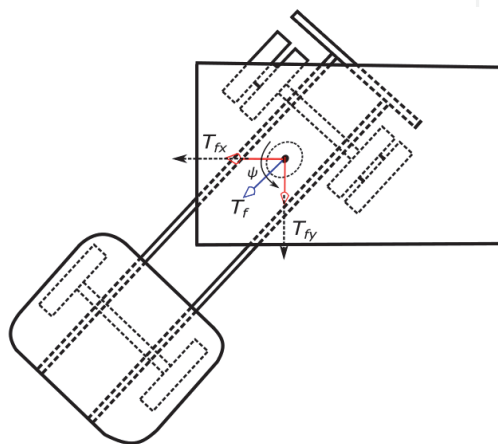


Figure 17.
 Torque components.

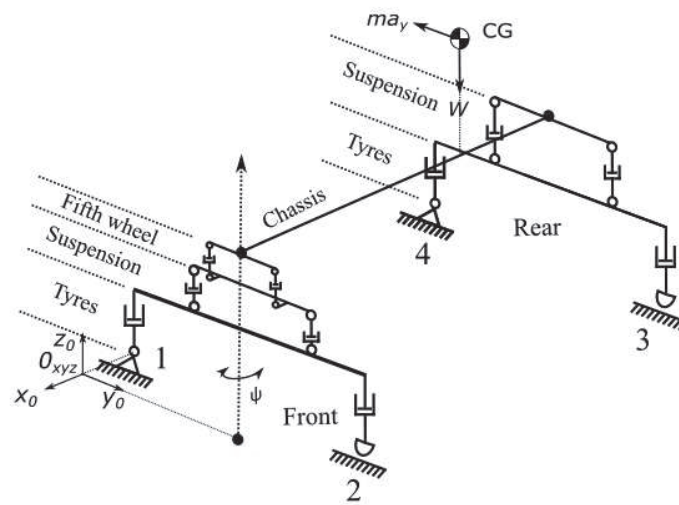


Figure 18.
Trailer model.

$$T_{fy} = T_f \cos \psi \quad (16)$$

where T_{fx} (T_{x28}) is the torque applied in the x -axis (this torque acts on the lateral load transfer on front axle), T_{fy} (T_{y28}) is the torque applied in the y -axis, and ψ is the steering angle of trailer front axle.

1.5 Three-dimensional trailer model

Considering the systems developed, the model of the trailer (**Figure 18**) is composed of the following mechanisms:

- the front mechanism of the trailer is composed for the tyres, the suspension, and the fifth wheel,
- the rear mechanism is composed for the tyres, and the suspension, and
- the last mechanism is the chassis and links the front and rear mechanism of the model.

The kinematic chain of the trailer model (**Figure 18**) is composed of 28 joints ($j = 28$; 14 revolute joints 'R', 10 prismatic joints 'P', 2 spherical joints 'S', 2 spherical slider joints 'S_d'), and 23 links ($n = 23$).

2. Static analysis of the mechanism

Several methodologies allow us to obtain a complete static analysis of the mechanism. For this purpose, the Davies method was used to analyse the mechanisms statically [11, 22–29]. This method was selected because it offers a straightforward way to obtain a static model of the mechanism, and this model can be easily adaptable using this approach.

2.1 External forces and load distribution

In the majority of LCVs, the load on the trailers is fixed and nominally centred; for this reason, the initial position lateral of the centre of gravity is centred and symmetric.

Usually, the national regulation boards establish the maximum load capacity of the axles of LCVs; this is based on the design load capacity of the pavement and bridges, so each country has its regulations. In this scope, the designers develop their products considering that the trailer is loaded uniformly, causing the axle's load distribution to be in accordance with the laws. **Figure 19** shows the example of the normal load distribution.

However, some loading does not properly distribute the load, which ultimately changes the centre of gravity of the trailer forwards or backwards, as shown in **Figure 20** respectively.

In **Figures 19** and **20**, F_f and F_r are the forces acting on the front and rear axles respectively.

Generally, the CG position is dependent on the type of cargo, and the load distribution on the trailer and it varies in three directions: longitudinal (x -axis), lateral (y -axis), and vertical (z -axis), as shown **Figure 21**.

Here, d_1 denotes the lateral CG displacement, d_2 denotes the longitudinal CG displacement, and d_3 the vertical CG displacement.

Furthermore, **Figure 22a** and **b** show that only the weight (W) and the lateral inertial force (ma_y) act on the trailer CG, but, when the model takes into account

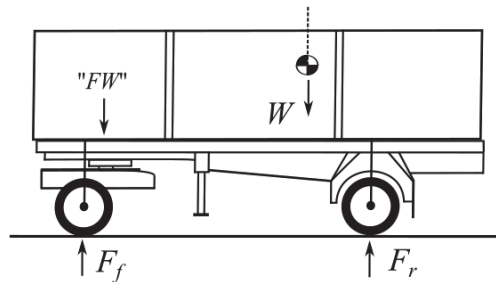


Figure 19.
Normal load distribution.

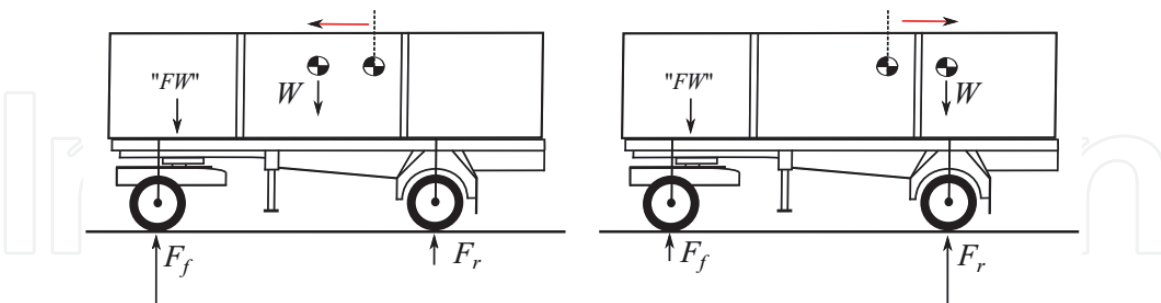


Figure 20.
Longitudinal CG movement.

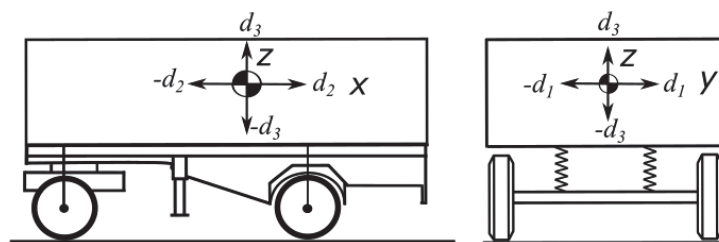
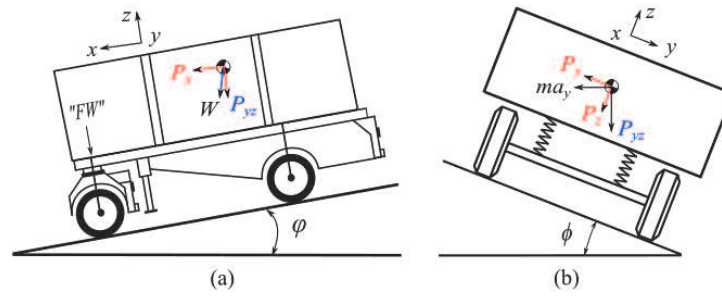


Figure 21.
CG displacements.


Figure 22.

(a) Longitudinal slope of the road. (b) Banked road.

the longitudinal slope angle (φ) and the bank angle (ϕ) of the road, these forces have three components, as represented in Eqs. (17)–(19).

$$P_x = W \sin \varphi \quad (17)$$

$$P_y = -W \sin \phi \cos \varphi + ma_y \cos \phi \quad (18)$$

$$P_z = W \cos \phi \cos \varphi + ma_y \sin \phi \quad (19)$$

where P_x is the force acting on the x -axis, P_y is the force acting on the y -axis, and P_z is the force acting on the z -axis.

Finally, the load distribution of the trailer on a road with a slope angle is given by the **Figure 23** and Eq. (20).

$$P_x h_2 - P_z (a \pm d_2) + F_r L = 0 \quad (20)$$

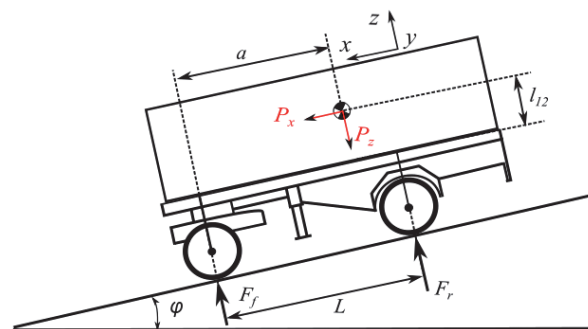
where h_2 is the instantaneous CG height, L is the wheelbase of the trailer, and a is the distance from the front axle to the centre of gravity.

2.2 Screw theory of the mechanism

Screw theory enables the representation of the mechanism's instantaneous position in a coordinate system (successive screw displacement method) and the representation of the forces and moments (wrench), replacing the traditional vector representation. All these fundamentals applied to the mechanism are briefly presented below.

2.2.1 Method of successive screw displacements of the mechanism

In the kinematic model for a mechanism, the successive screws displacement method is used. **Figures 24–28** and **Table 1** present the screw parameters of the mechanism.


Figure 23.

Load distribution of a trailer on a road with slope angle.

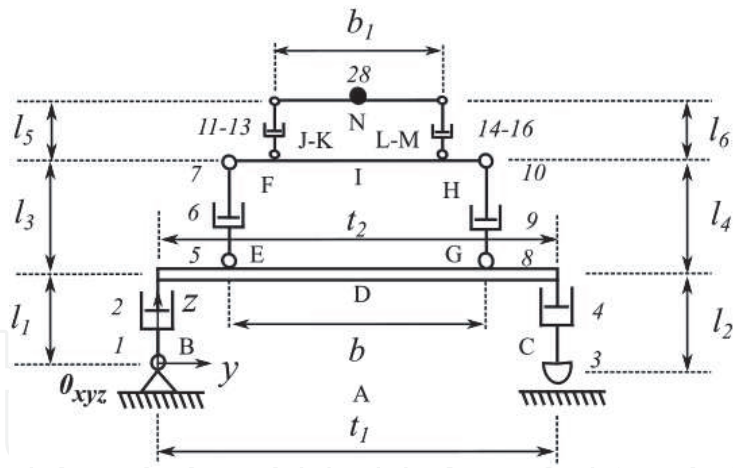


Figure 24.
 Variables of the mechanism position (model of the front of the trailer).

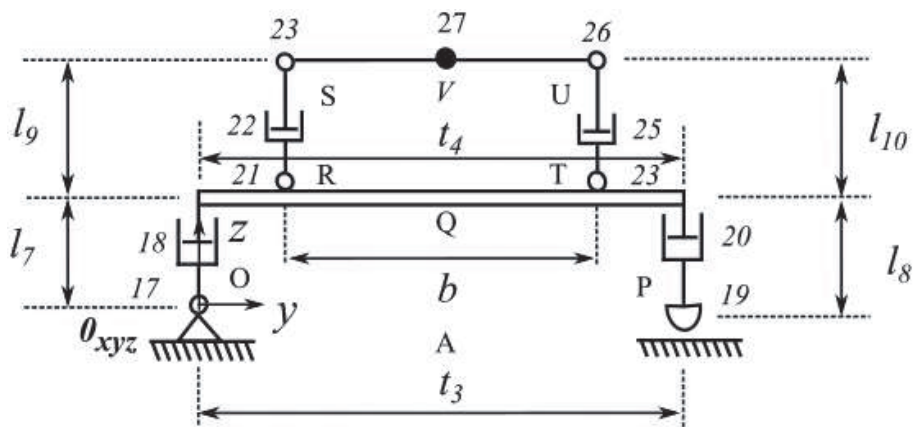


Figure 25.
 Variables of the mechanism position (model of the rear of the trailer).

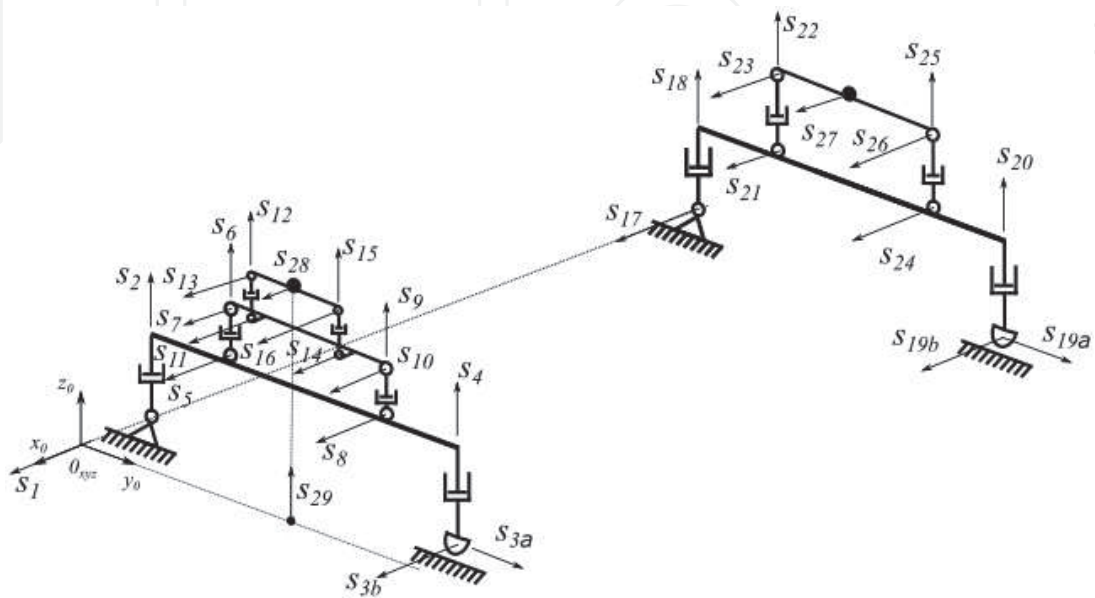


Figure 26.
 Vector along the direction of the screws axis (model of the front and rear of the trailer).

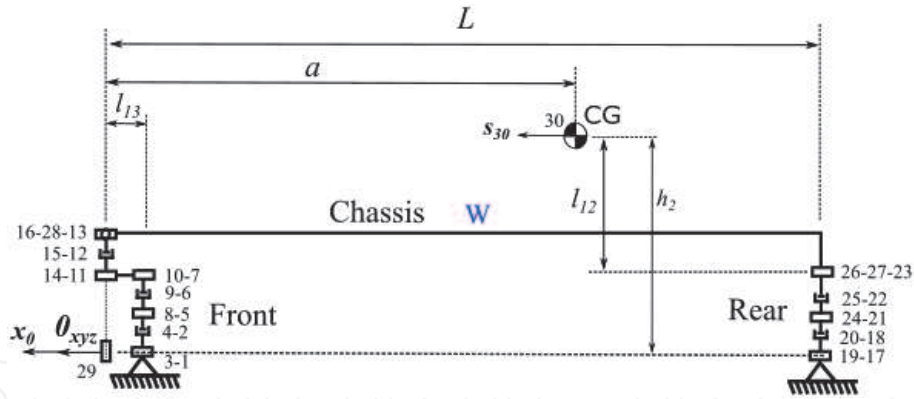


Figure 27.
Variables of the mechanism position (side view of the trailer).

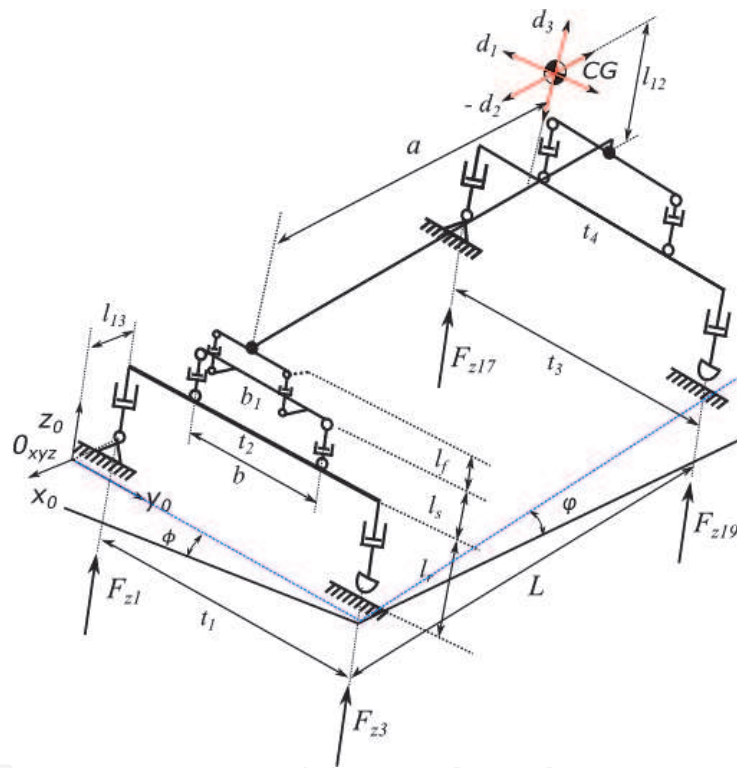


Figure 28.
Variables of the mechanism position (three-dimensional model).

In **Figures 24–28** and **Table 1**, l_{13} is the distance between the fifth wheel and the front axle, $l_{1;2;7;8}$ are the dynamic rolling radii of tyres, $t_{1;3}$ are the front and rear track widths of the trailer respectively, $t_{2;4}$ are the front and rear axle widths respectively, b is the lateral separation between the springs, b_1 is the fifth wheel width, θ_i is the revolution joint angle rotation i , $l_{3;4;9;10}$ are the instantaneous heights of the leaf spring, l_{12} is the height of CG above the chassis, and ψ is the trailer/trailer angle.

This method enables the determination of the displacement of the mechanism and the instantaneous position vector s_{0i} of the joints, and the centre of gravity (The vector s_{0i} (**Table 2**) is obtained from the first three terms of the last column of equations shown in **Table 3**).

2.2.2 Wrench—Forces and moments

In the static analysis, all forces and moments of the mechanism are represented by wrenches ($\A) [13]. The wrenches applied can be represented by the

Joints and points	s			s_0			θ	d
Joint 1	1	0	0	$-l_{13}$	0	0	θ_1	0
Joint 2	0	0	1	$-l_{13}$	0	0	0	l_1
Joint 3a	0	1	0	$-l_{13}$	0	0	0	t_1
Joint 3b	1	0	0	$-l_{13}$	0	0	θ_3	0
Joint 4	0	0	1	$-l_{13}$	0	0	0	l_2
Joint 5	1	0	0	$-l_{13}$	$(t_2 - b)/2$	0	θ_5	0
Joint 6	0	0	1	$-l_{13}$	$(t_2 - b)/2$	0	0	l_3
Joint 7	1	0	0	$-l_{13}$	$(t_2 - b)/2$	0	θ_7	0
Joint 8	1	0	0	$-l_{13}$	$(t_2 + b)/2$	0	θ_8	0
Joint 9	0	0	1	$-l_{13}$	$(t_2 + b)/2$	0	0	l_4
Joint 10	1	0	0	$-l_{13}$	$(t_2 + b)/2$	0	θ_{10}	0
Joint 11	1	0	0	0	$(t_2 - b_1)/2$	0	θ_{11}	0
Joint 12	0	0	1	0	$(t_2 - b_1)/2$	0	0	l_5
Joint 13	1	0	0	0	$(t_2 - b_1)/2$	0	θ_{13}	0
Joint 14	1	0	0	0	$(t_2 + b_1)/2$	0	θ_{14}	0
Joint 15	0	0	1	0	$(t_2 + b_1)/2$	0	0	l_6
Joint 16	1	0	0	0	$(t_2 + b_1)/2$	0	θ_{16}	0
Joint 17	1	0	0	$-L$	0	0	θ_{17}	0
Joint 18	0	0	1	$-L$	0	0	0	l_7
Joint 19a	0	1	0	$-L$	0	0	0	t_3
Joint 19b	1	0	0	$-L$	0	0	θ_{19}	0
Joint 20	0	0	1	$-L$	0	0	0	l_8
Joint 21	1	0	0	$-L$	$(t_4 - b)/2$	0	θ_{21}	0
Joint 22	0	0	1	$-L$	$(t_4 - b)/2$	0	0	l_9
Joint 23	1	0	0	$-L$	$(t_4 - b)/2$	0	θ_{23}	0
Joint 24	1	0	0	$-L$	$(t_4 + b)/2$	0	θ_{24}	0
Joint 25	0	0	1	$-L$	$(t_4 + b)/2$	0	0	l_{10}
Joint 26	1	0	0	$-L$	$(t_4 + b)/2$	0	θ_{26}	0
Joint 27	1	0	0	$-L$	$t_4/2$	0	θ_{27}	0
Joint 28	1	0	0	0	$t_2/2$	0	θ_{28}	0
Point 29	0	0	1	0	$t_2/2$	0	ψ	0
CG (30)	1	0	0	$-a \pm d_2$	$(t_4/2) \pm d_1$	$l_{12} \pm d_3$	0	0

Table 1.
 Screw parameters of the mechanism.

vector $\$^A = [M_x M_y M_z F_x F_y F_z]^T$, where F denotes the forces, and M denotes the moments.

To simplify the model of **Figure 28**, the following considerations were made:

- for the x -direction a steady-state model was used in the analysis;
- disturbances imposed by the road and the lateral friction forces (F_y) (tyre-ground contact) in the joints 3 and 19 were neglected; and

References	s_{oi}		
1	$\frac{t_2 s_{29} - 2l_{13} c_{29}}{2}$	$-\frac{2l_{13} s_{29} + t_2 c_{29} - t_2}{2}$	0
2	$\frac{(2l_1 s_1 + t_2) s_{29} - 2l_{13} c_{29}}{2}$	$-\frac{(2l_1 s_1 + t_2) c_{29} + 2l_{13} s_{29} - t_2}{2}$	$l_1 c_1$
3	$\frac{(t_2 - 2l_1) s_{29} - 2l_{13} c_{29}}{2}$	$-\frac{2l_{13} s_{29} + (t_2 - 2l_1) c_{29} - t_2}{2}$	0
4	$\frac{(2l_2 s_3 + t_2 - 2l_1) s_{29} - 2l_{13} c_{29}}{2}$	$-\frac{2l_{13} s_{29} + (2l_2 s_3 + t_2 - 2l_1) c_{29} - t_2}{2}$	$l_2 c_3$
5-16	\vdots	\vdots	\vdots
17	$-L$	0	0
18	$-L$	$-l_7 s_{17}$	$l_7 c_{17}$
19	$-L$	t_3	0
20	$-L$	$t_3 - l_8 s_{19}$	$l_8 c_{19}$
21	$-L$	$-\frac{2l_{17} s_{17} + (b_2 - t_4) c_{17}}{2}$	$\frac{(t_4 - b_2) s_{17} + 2l_{17} c_{17}}{2}$
22-23	$-L$	$-\frac{2l_{17} s_{17} + (b_2 - t_4) c_{17} + 2l_9 s_{21+17}}{2}$	$\frac{(t_4 - b_2) s_{17} + 2l_{17} c_{17} + 2l_9 c_{21+17}}{2}$
24-28	\vdots	\vdots	\vdots
CG	$-a \pm d_2$	$*h_1$	$*h_2$

$s_i = \sin \theta_i c_i = \cos \theta_i$
 $*h_1 = -\frac{(2l_{12} \pm 2d_3) s_{27+23+21+17} \pm d_1 c_{27+23+21+17} - b_2 c_{23+21+17} + 2l_9 s_{21+17} + 2l_7 s_{17} + (b_2 - t_4) c_{17}}{2}$
 $*h_2 = -\frac{\pm d_1 s_{27+23+21+17} + (\pm 2d_3 - 2l_{12}) c_{27+23+21+17} - b_2 s_{23+21+17} - 2l_9 c_{21+17} - 2l_7 c_{17} + (b_2 - t_4) s_{17}}{2}$

Table 2.
Instantaneous position vector s_{oi} .

Joints and points	Instantaneous position matrix
Joint 1	$p'_1 = A_{29} A_1 p_1$
Joint 2	$p'_2 = A_{29} A_1 A_2 p_2$
Joint 3	$p'_3 = A_{29} A_{3a} A_{3b} p_3$
Joint 4	$p'_4 = A_{29} A_{3a} A_{3b} A_4 p_4$
Joint 5	$p'_5 = A_{29} A_1 A_2 A_5 p_5$
Joint 6	$p'_6 = A_{29} A_1 A_2 A_5 A_6 p_6$
Joint 7	$p'_7 = A_{29} A_1 A_2 A_5 A_6 A_7 p_7$
Joint 8	$p'_8 = A_{29} A_1 A_2 A_8 p_8$
Joint 9	$p'_9 = A_{29} A_1 A_2 A_8 A_9 p_9$
Joint 10	$p'_{10} = A_{29} A_1 A_2 A_8 A_9 A_{10} p_{10}$
Joint 11	$p'_{11} = A_{29} A_1 A_2 A_5 A_6 A_7 A_{11} p_{11}$
Joint 12	$p'_{12} = A_{29} A_1 A_2 A_5 A_6 A_7 A_{11} A_{12} p_{12}$
Joint 13	$p'_{13} = A_{29} A_1 A_2 A_5 A_6 A_7 A_{11} A_{12} A_{13} p_{13}$
Joint 14	$p'_{14} = A_{29} A_1 A_2 A_5 A_6 A_7 A_{14} p_{14}$
Joint 15	$p'_{15} = A_{29} A_1 A_2 A_5 A_6 A_7 A_{14} A_{15} p_{15}$
Joint 16	$p'_{16} = A_{29} A_1 A_2 A_5 A_6 A_7 A_{14} A_{15} A_{16} p_{16}$
Joint 17	$p'_{17} = A_{17} p_{17}$
Joint 18	$p'_{18} = A_{17} A_{18} p_{18}$
Joint 19	$p'_{19} = A_{19a} A_{19b} p_{19}$

Joints and points	Instantaneous position matrix
Joint 20	$p'_{20} = A_{19a} A_{19b} A_{20} p_{20}$
Joint 21	$p'_{21} = A_{17} A_{18} A_{21} p_{21}$
Joint 22	$p'_{22} = A_{17} A_{18} A_{21} A_{22} p_{22}$
Joint 23	$p'_{23} = A_{17} A_{18} A_{21} A_{22} A_{23} p_{23}$
Joint 24	$p'_{24} = A_{17} A_{18} A_{24} p_{24}$
Joint 25	$p'_{25} = A_{17} A_{18} A_{24} A_{25} p_{25}$
Joint 26	$p'_{26} = A_{17} A_{18} A_{24} A_{25} A_{26} p_{26}$
Joint 27	$p'_{27} = A_{17} A_{18} A_{21} A_{22} A_{23} A_{27} p_{27}$
Joint 28	$p'_{28} = A_{29} A_1 A_2 A_5 A_6 A_7 A_{11} A_{12} A_{13} A_{28} p_{28}$
CG (30)	$p'_{CG} = A_{17} A_{18} A_{21} A_{22} A_{23} A_{27} A_{CG} p_{CG}$

Table 3.
 Instantaneous position matrix.

Joints and reference points	Constraints and forces	s_i			Inst. position vector s_{0i}
Revolute joints 1, 7, 8, 10, 13, 14, 16, 17, 23, 24, and 26	F_{xi}	1	0	0	Revolute joints 1, 7, 8, 10, 13, 14, 16, 17, 23, 24, and 26
	F_{yi}	0	1	0	
	F_{zi}	0	0	1	
	M_{yi}	0	1	0	
	M_{zi}	0	0	1	
Spherical slider joints 3 and 19	F_{xi}	1	0	0	Spherical slider joints 3 and 19
	F_{zi}	0	0	1	
Revolute joints 5, 11, and 21	F_{xi}	1	0	0	Revolute joints 5, 11, and 21
	F_{yi}	0	1	0	
	F_{zi}	0	0	1	
	T_{xi}	1	0	0	
	M_{yi}	0	1	0	
	M_{zi}	0	0	1	
Prismatic joints 2, 4, 6, 9, 12, 15, 18, 20, 22 and 25	F_{xi}	1	0	0	Prismatic joints 2, 4, 6, 9, 12, 15, 18, 20, 22, and 25
	F_{ni}	0	$\cos \theta_{i-1}$	$\sin \theta_{i-1}$	
	M_{xi}	1	0	0	
	M_{yi}	0	1	0	
	M_{zi}	0	0	1	
Prismatic joints 2, 4, 18, and 20	F_{Ti}	0	$-\sin \theta_{i-1}$	$\cos \theta_{i-1}$	Prismatic joints 2, 4, 18, and 20
Prismatic joints 6, 9, 22, and 25	F_{LSi}	0	$-\sin \theta_{i-1}$	$\cos \theta_{i-1}$	Prismatic joints 6, 9, 22, and 25
Prismatic joints 12 and 15	F_{FWi}	0	$-\sin \theta_{i-1}$	$\cos \theta_{i-1}$	Prismatic joints 12 and 15

Joints and reference points	Constraints and forces		s_i		Inst. position vector s_{0i}
Spherical joints 27 and 28	F_{xi}	1	0	0	Spherical joints 27 and 28
	F_{yi}	0	1	0	
	F_{zi}	0	0	1	
	T_{xi}	1	0	0	
CG (30)	P_x	1	0	0	CG (30)
	P_y	0	-1	0	
	P_z	0	0	-1	

Table 4.
Wrench parameters of the mechanism.

- the components of the trailer weight (W) and the inertial force (ma_y) are the only external forces acting on the trailer CG.

Considering a static analysis in a three-dimensional space [7], the corresponding wrenches of each joint and external forces are defined by the parameters of **Table 4**, where s_i represents the orientation vector of each wrench i .

All of the wrenches of the mechanism together comprise the action matrix $[A_d]$ given by Eq. (21) (or the amplified matrix of the Eq. (22)).

$$[A_d]_{6 \times 148} = \begin{bmatrix} \$F_{x1}^A & \$F_{y1}^A & \$F_{z1}^A & \cdots & \$P_x^A & \$P_y^A & \$P_z^A \end{bmatrix} \quad (21)$$

$$[A_d] = \begin{bmatrix} 0 & 0 & -p_1 F_{z1} & \cdots & 0 & h_2 P_y & -h_1 P_z \\ 0 & 0 & -p_2 F_{z1} & \cdots & h_2 P_x & 0 & (-a \pm d_2) P_z \\ p_1 F_{x1} & p_2 F_{y1} & 0 & \cdots & -h_1 P_x & -(-a \pm d_2) P_y & 0 \\ F_{x1} & 0 & 0 & \cdots & P_x & 0 & 0 \\ 0 & F_{y1} & 0 & \cdots & 0 & -P_y & 0 \\ 0 & 0 & F_{z1} & \cdots & 0 & 0 & -P_z \end{bmatrix} \quad (22)$$

where p_i is a system variable.

The wrench can be represented by a normalised wrench and a magnitude. Therefore, from the Eq. (22) the unit action matrix and the magnitudes action vector are obtained, as represented by Eqs. (23) and (24).

$$[\hat{A}_d]_{6 \times 148} = \begin{bmatrix} 0 & 0 & -p_1 & \cdots & 0 & h_2 & -h_1 \\ 0 & 0 & -p_2 & \cdots & h_2 & 0 & (-a \pm d_2) \\ p_1 & p_2 & 0 & \cdots & -h_1 & -(-a \pm d_2) & 0 \\ 1 & 0 & 0 & \cdots & 1 & 0 & 0 \\ 0 & 1 & 0 & \cdots & 0 & -1 & 0 \\ 0 & 0 & 1 & \cdots & 0 & 0 & -1 \end{bmatrix} \quad (23)$$

$$[\Psi]_{148 \times 1} = [F_{x1} \quad F_{y1} \quad F_{z1} \quad \cdots \quad P_x \quad P_y \quad P_z] \quad (24)$$

2.2.3 Graph theory

Kinematic chains and mechanisms are comprised of links and joints, which can be represented by graphs, where the vertices correspond to the links, and the edges correspond to the joints and external forces [5, 7].

The mechanism of the **Figure 28** is represented by the direct coupling graph of the **Figure 29**. This graph has 23 vertices (links) and 31 edges (joints and external forces (P_x , P_y , and P_z)).

The direct coupling graph (**Figure 29**) can be represented by the incidence matrix $[I]_{23 \times 31}$ [30] (Eq. (25)). The incidence matrix provides the mechanism cut-set matrix $[Q]_{22 \times 31}$ [11, 25–28, 30] (Eq. (26)) for the mechanism, where each line represents a cut graph and the columns represent the mechanism joints. Besides, this matrix is rearranged, allowing 22 branches (edges 1–3, 5–9, 11–15, 17–19, 21–25, and 27—identity matrix) and 9 chords (edges 4, 10, 16, 20, 26, 28, P_x , P_y , and P_z) to be defined, as shown in **Figure 30**.

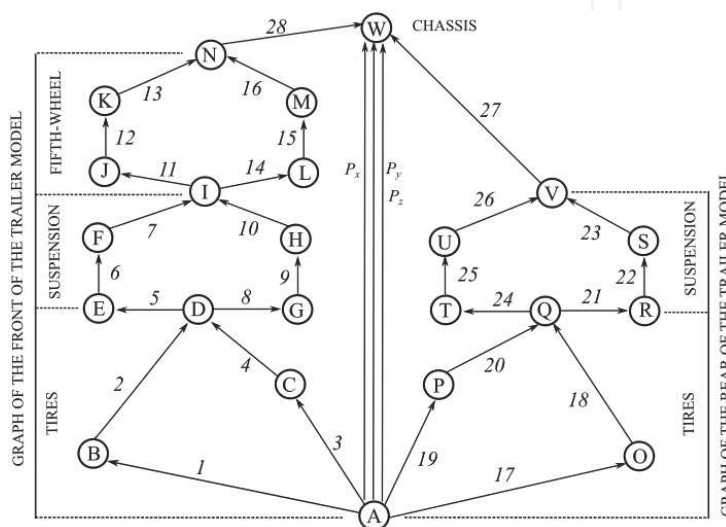


Figure 29.
 Direct coupling graph of the mechanism.

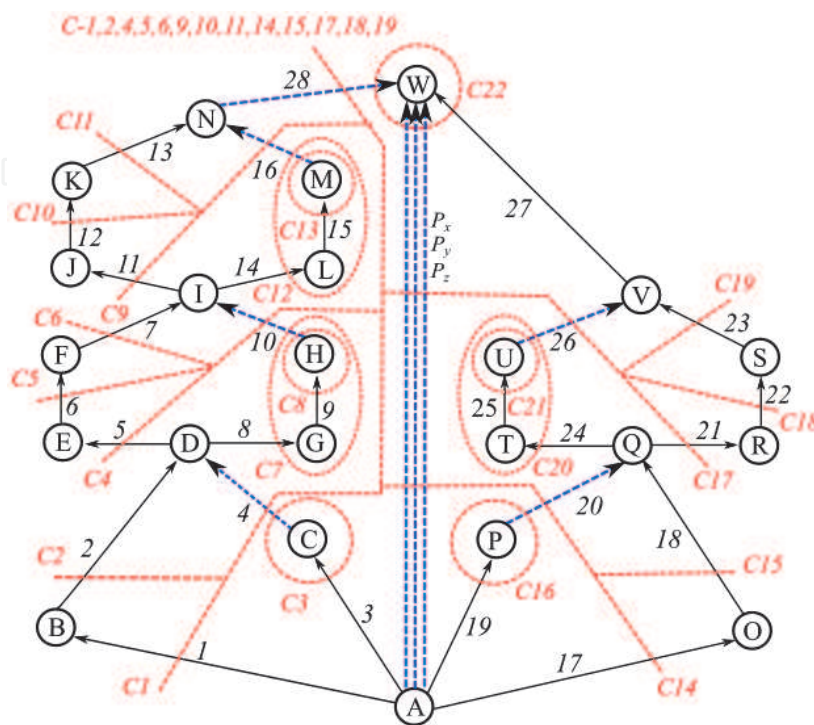


Figure 30.
 Cut-set action graph of the mechanism.

replacing P_y and P_z :

$$\begin{aligned}
 & F_{z3} + \frac{P_1 + t_3}{t_1 \cos \psi} F_{z19} + \frac{P_1}{t_1 \cos \psi} F_{z17} \\
 & - \frac{h_1 + P_1}{t_1 \cos \psi} (W \cos \phi \cos \varphi + m a_y \sin \phi) \\
 & + \frac{h_2}{t_1 \cos \psi} (m a_y \cos \phi - W \sin \phi \cos \varphi) = 0
 \end{aligned} \quad (34)$$

where P_1 is a system variable ($P_1 = (2l_{13} \sin \psi + t_2 (\cos \psi - 1))/2$), h_1 is the instantaneous lateral distance between the zero-reference frame and the centre of gravity, and h_2 is the instantaneous CG height (**Table 2**). Simplifying the equation, and making $\tan(\phi) = e$, where e is the tangent of the bank angle, we have:

$$\begin{aligned}
 \frac{a_y}{g} &= \frac{h_1 \cos \varphi + h_2 e \cos \varphi}{h_2 - (h_1 + P_1)e} \times \\
 & \left(1 - \frac{t_1 F_{z3} \cos \psi + P_1 (F_{z17} - W \cos \phi \cos \varphi) + (P_1 + t_3) F_{z19}}{W \cos \phi (h_1 \cos \varphi + h_2 e \cos \varphi)} \right)
 \end{aligned} \quad (35)$$

According to the static redundancy problem known as the four-legged table [31, 32], a plane is defined by just three points in space and, consequently, a four-legged table has support plane multiplicities. This is why when one leg loses contact with the ground, the table is supported by the other three, as shown in **Figure 31**.

The problem of the four-legged table is observed in dynamic rollover tests when the rear inner tyre loses contact with the ground ($F_{z19} = 0$), and the front inner tyre (F_{z3}) does not, as shown, for example, in **Figure 32**.

Applying this theory to the vehicle stability, when a vehicle makes a turn, it is subjected to an increasing lateral load until it reaches the rollover threshold [32]. During the turning, the rear inner tyre is usually the one that loses contact with the ground. For this condition ($F_{z19} = 0$), and thus:

$$\begin{aligned}
 SRT_{3D_{\psi\phi\varphi}} &= \frac{h_1 \cos \varphi + h_2 e \cos \varphi}{h_2 - (h_1 + P_1)e} \times \\
 & \left(1 - \frac{t_1 F_{z3} \cos \psi + P_1 (F_{z17} - W \cos \phi \cos \varphi)}{W \cos \phi (h_1 \cos \varphi + h_2 e \cos \varphi)} \right)
 \end{aligned} \quad (36)$$

where $SRT_{3D_{\psi\phi\varphi}}$ factor is the three-dimensional static rollover threshold for a trailer model with trailer/trailer angle (ψ), bank angle (e), and slope angle (φ).

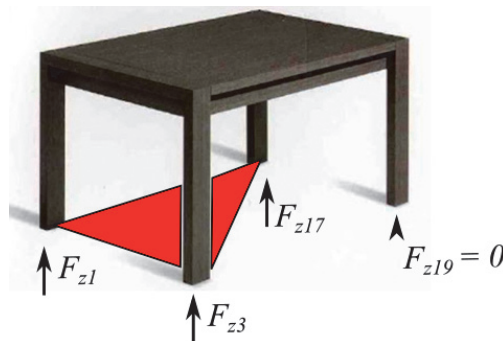


Figure 31.
Redundancy problem of the four-legged table.



Figure 32.
 Dynamic rollover test. Source: Adapted of Cabral [33].

The normal forces F_{z3} and F_{z17} depend on the *LLT* coefficient in the front and rear axles respectively [4, 21, 34]. Furthermore, this coefficient depends on the vehicle type, speed, suspension, tyres, etc.

This information demonstrates that the $SRT_{3D_{\psi\phi\phi}}$ factor of a vehicle (Eq. (36)) is, in general, inferior to the *SRT* factor for a two-dimensional model vehicle [35], as shown in Eq. (37).

$$SRT_{2D} = \frac{a_y}{g} = \frac{t}{2h} \quad (37)$$

where h is the *CG* height, t is the vehicle track.

Parameters of the trailer	Value	Units
Trailer weight— W	355.22	kN
Front and rear track widths ($t_{1,3}$)	1.86	m
Front and rear axles widths ($t_{2,4}$)	1.86	m
Stiffness of the suspension per axle (k_s) [37]	1800	kN.m ⁻¹
Number of axles at the front (trailer) (four tyres per axle)	2	
Number of axles at the rear (trailer) (four tyres per axle)	3	
Vertical stiffness per tyre (k_T) ([37])	840	kN.m ⁻¹
Initial suspension height ($l_{3,4,9,10}$) (l_s)	0.205	m
Initial dynamic rolling radius ($l_{1,2,7,8}$) (l_r) (Michelin XZA® [36])	0.499	m
Initial height of the fifth wheel (l_{fi})	0.1	m
Lateral separation between the springs (b)	0.95	m
Fifth wheel width (b_1)	0.6	m
<i>CG</i> height above the chassis (l_{12})	1.346	m
Distance between the fifth wheel and the front axle (l_{13})	0.15	m
Wheelbase of the trailer (L)	4.26	m
Distance from the front axle to the centre of gravity (a)	3	m
Offset of the cargo d_1	0.1	m
Trailer/trailer angle (ψ)	0	°

Table 5.
 Parameters of the trailer model.

With Eq. (36), it is possible to obtain a better vehicle stability representation and the $SRT_{3D_{\psi\phi\varphi}}$ factor value attainments closer to reality.

To simplify the solution of the system of equations in Eq. (30), the following hypotheses were considered:

- in the majority of LCVs, the load on the trailers is uniformly distributed (Eq. (20));
- the lateral load transfer of the trailer model is controlled through the torsional moment of the chassis (spherical joints 27 and 28 (Eqs. (15) and (16))).

Eq. (38) shows the final static system for the stability analysis, solving this system using the Gauss-Jordan elimination method, all secondary variables are a function of primary variables, (P_x —force acting on the x -axis, P_y —force acting on the y -axis, and P_z —force acting on the z -axis).

$$\begin{array}{l}
 \text{Cut 1} \\
 \vdots \\
 \text{Cut 22} \\
 \text{Eq. (20)} \\
 \text{Eq. (15)} \\
 \text{Eq. (16)}
 \end{array}
 \begin{bmatrix}
 0 & 0 & \dots & 0 & 0 & -p_1 & 0 & 0 & 0 & 0 & 0 & 0 \\
 0 & 0 & \dots & 0 & 0 & -p_2 & 0 & 0 & 0 & 0 & 0 & 0 \\
 p_1 & p_2 & \dots & 0 & 0 & 0 & 0 & 0 & 0 & 0 & 0 & 0 \\
 1 & 0 & \dots & 0 & 0 & 0 & 0 & 0 & 0 & 0 & 0 & 0 \\
 0 & 1 & \dots & 0 & 0 & 0 & 0 & 0 & 0 & 0 & 0 & 0 \\
 0 & 0 & \dots & 0 & 0 & 1 & 0 & 0 & 0 & 0 & 0 & 0 \\
 \vdots & \vdots \\
 0 & 0 & \dots & 0 & 0 & 0 & 0 & 0 & 0 & 0 & h_2 & -h_1 \\
 0 & 0 & \dots & 0 & 0 & 0 & 0 & 0 & 0 & h_2 & 0 & (-a \pm d_2) \\
 0 & 0 & \dots & 0 & 0 & 0 & 0 & 0 & 0 & -h_1 & -(-a \pm d_2) & 0 \\
 0 & 0 & \dots & 0 & 0 & 0 & 0 & 0 & 0 & 1 & 0 & 0 \\
 0 & 0 & \dots & 0 & 0 & 0 & 0 & 0 & 0 & 0 & -1 & 0 \\
 0 & 0 & \dots & 0 & 0 & 0 & 0 & 0 & 0 & 0 & 0 & -1 \\
 0 & 0 & \dots & 0 & 0 & 0 & 0 & L & L & h_2 & 0 & -(-a \pm d_2) \\
 0 & 0 & \dots & 0 & 0 & 0 & 0 & 0 & 0 & 0 & 0 & 0 \\
 0 & 0 & \dots & 0 & 0 & 0 & 0 & 0 & 0 & 0 & 0 & 0
 \end{bmatrix}
 \cdot
 \begin{bmatrix}
 F_{x1} \\
 F_{y1} \\
 \vdots \\
 T_{x5} \\
 T_{x11} \\
 T_{x21} \\
 T_{x27} \\
 T_{x28} \\
 F_{T2} \\
 F_{T4} \\
 F_{T18} \\
 F_{T20} \\
 F_{LS6} \\
 F_{LS9} \\
 F_{LS22} \\
 F_{LS25} \\
 F_{FW12} \\
 F_{FW17} \\
 F_{z1} \\
 F_{z3} \\
 F_{z19} \\
 F_{z17} \\
 P_x \\
 P_y \\
 P_z
 \end{bmatrix}
 = [0]_{135 \times 1}
 \tag{38}$$

3. Case study

In this study, a B-train trailer with two axles on front and three axles on the rear is analysed. This model has a suspension system with a tandem axle, and its parameters depend on the construction materials. Another important parameter of the model is the dynamic rolling radius or loaded radius l_i . The proposed model considers Michelin XZA® [36] radial tyres. **Table 5** shows the parameters of the trailer used in this analysis [32, 38].

To calculate the *SRT* factor, the inertial force is increased until the lateral load transfer in the rear axle is complete (the entire load is transferred from the rear inner tyre to the rear outer tyre when the model makes a turn). The reduction in the *SRT* factor (Eq. (36) and the solution of the system of Eq. (38)) results from the combined action of the trailer systems, which allows a body roll angle of the trailer model (**Figure 33**) [32]. In this figure, it can be seen how the stability factor varies according to the influence of some of the parameters of the developed model.

When the model considers all parameters, the *LLT* coefficient on the front axle is approximately 70% of the *LLT* coefficient on the rear axle [21]. Applying this concept, the SRT_{all} factor reduces to $0.3364 g$. Finally, the proposed model shows how the lateral offset of the cargo ($d_1 = 0.1 m$) influences the SRT_{off} factor: 2 cm of lateral offset corresponds to a loss of stability of around $0.01 g$ a reduction similar to that reported by Winkler [20, 32].

Additionally, the proposed model shows how a change in the lateral separation between the springs (b) influences the *SRT* factor. Some *LCVs* with tanker trailers have a greater lateral separation between the springs, which leads to a decrease in the roll angle and thus an increase in the *SRT* factor: 1 cm of lateral separation between the springs corresponds to a gain or loss of stability of around $0.001 g$, as shown in **Figure 33b** [32].

This model also allows the determination of the lateral (h_1) and vertical (h_2) *CG* location (**Figure 34**).

Finally, if we consider the recommended maximum lateral load transfer ratio for the rear axle of 0.6 [39, 40], and also include the recommended bank angle and longitudinal slope of the road [41, 42], we can calculate the *SRT* factor for a trailer model on downhill and uphill corners. **Table 6** shows a trailer model with different trailer/trailer angles (ψ) [32].

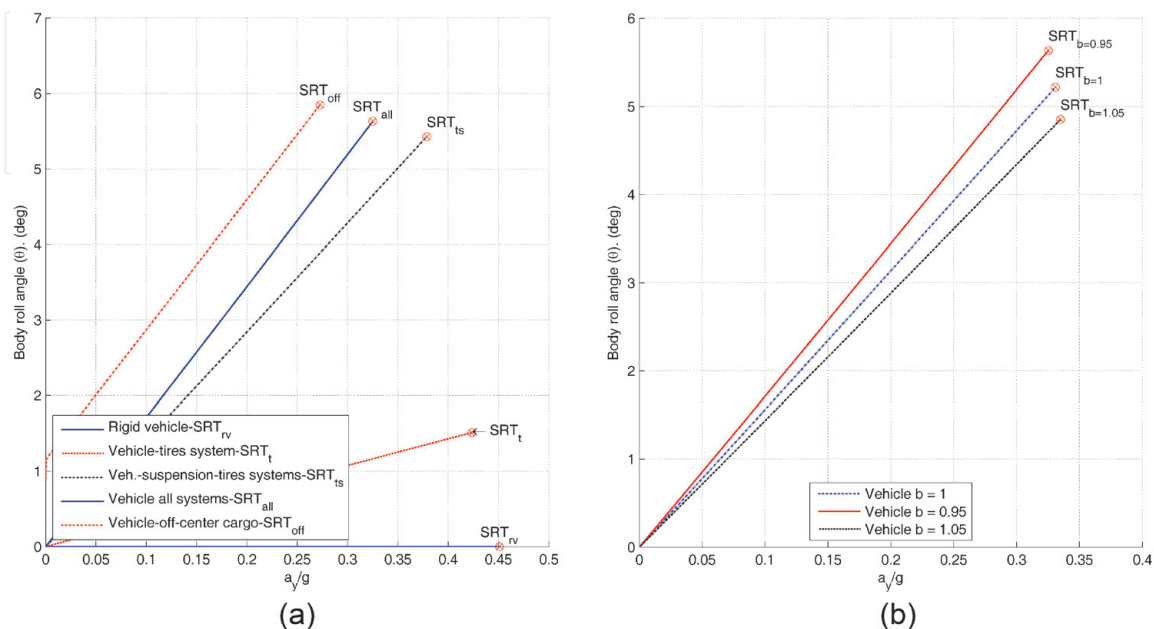


Figure 33.
 (a) Roll angle of the trailer (θ). (b) Change in the *SRT* factor.

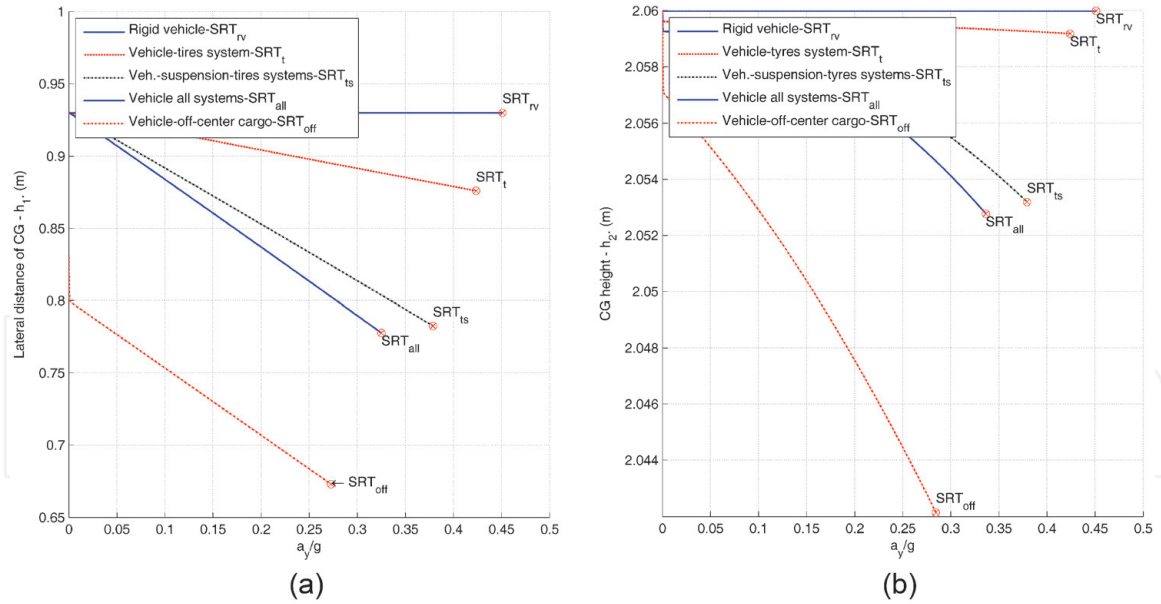


Figure 34.
(a) Lateral CG location. (b) Vertical CG location.

Slope angle (φ)-(%)		Uphill corners					Downhill corners			
Trailer/trailer angle (ψ)-($^{\circ}$)	Bank angle (ϕ)-(%)	8	6	4	2	0	2	4	6	8
0	0	0.240	0.223	0.214	0.208	0.202	0.198	0.194	0.190	0.186
0	2	0.261	0.245	0.235	0.228	0.223	0.218	0.214	0.210	0.206
0	4	0.283	0.265	0.256	0.249	0.244	0.239	0.234	0.230	0.226
0	6	0.305	0.286	0.277	0.270	0.265	0.260	0.256	0.252	0.248
0	8	0.327	0.308	0.299	0.292	0.285	0.281	0.276	0.272	0.268
0	10	0.350	0.330	0.320	0.313	0.307	0.303	0.298	0.294	0.290
10	0	0.241	0.223	0.214	0.207	0.202	0.197	0.193	0.189	0.185
10	2	0.262	0.245	0.234	0.227	0.222	0.217	0.213	0.209	0.205
10	4	0.283	0.265	0.256	0.249	0.243	0.239	0.233	0.229	0.225
10	6	0.306	0.286	0.276	0.270	0.264	0.259	0.255	0.251	0.247
10	8	0.328	0.308	0.298	0.291	0.285	0.280	0.276	0.271	0.267
10	10	0.351	0.330	0.319	0.312	0.307	0.302	0.297	0.293	0.288
20	0	0.241	0.222	0.212	0.206	0.200	0.195	0.191	0.187	0.182
20	2	0.262	0.244	0.233	0.226	0.220	0.216	0.211	0.207	0.203
20	4	0.283	0.264	0.254	0.247	0.242	0.236	0.232	0.227	0.224
20	6	0.306	0.285	0.275	0.268	0.262	0.257	0.253	0.249	0.245
20	8	0.328	0.307	0.297	0.290	0.283	0.278	0.274	0.270	0.265
20	10	0.351	0.329	0.318	0.311	0.305	0.300	0.295	0.291	0.286

Table 6.
Static rollover threshold (SRT) of the trailer model with trailer/trailer angle.

In the worst-case scenario, the trailer model, for a downhill corner with a bank angle of 0%, the longitudinal slope of the road of 8%, and a trailer/trailer angle of 20° can reduce the SRT factor of the model by 59.6%, using 0.4511 g as a reference [32].

An analysis of **Table 6** leads to the following conclusions for the critical conditions of the trailer:

- a 1% bank angle corresponds to gain in the stability of around 0.01 g ;
- when the trailer is in downhill corners, a 1% slope angle corresponds to a loss of stability of around 0.0021 g ;
- the trailer/trailer angle is inversely proportional to the *SRT* factor since when the trailer makes a horizontal curve with a small radio, and the trailer/trailer angle and inertial force are large, the *SRT* factor is lower.

4. Conclusions

This study demonstrates that the longitudinal characteristics of a trailer model have an essential influence on the *SRT* factor calculation. In this case, the *SRT* factor is approximately 38% lower than the previously reported standard value. This value is very close to that reported by Winkler [20] (i.e. 40%), which suggests that the proposed model provides consistent results [32].

This model also shows that the change in the lateral separation between the springs (b) plays an important role, and thus it should be considered in the design and construction of trailers. Greater lateral separation between the springs will increase the trailer model stability [32].

We also found that the parameters of the road, such as the bank angle and the longitudinal slope angle, can affect vehicle stability. This situation is closer to the actual problem: when the road is not planar, the lateral and the longitudinal load transfer play an important role in reducing the stability. On the other hand, this provides a very important warning, because some simplifications carried out when estimating the *SRT* factor can lead to a considerably higher stability value. This is a point of concern, leading to the perception that our roads are safer than they really are [32].

IntechOpen

Author details

Gonzalo Guillermo Moreno Contreras^{1,2*}, Rodrigo de Souza Vieira²
and Daniel Martins²

1 Mechanical Engineering Department, University of Pamplona, Colombia

2 Mechanical Engineering Department, Federal University of Santa Catarina
(UFSC), Brazil

*Address all correspondence to: gmoren@unipamplona.edu.co;
gmoren@hotmail.com

IntechOpen

© 2020 The Author(s). Licensee IntechOpen. This chapter is distributed under the terms of the Creative Commons Attribution License (<http://creativecommons.org/licenses/by/3.0>), which permits unrestricted use, distribution, and reproduction in any medium, provided the original work is properly cited. 

References

- [1] Rempel MR. Improving the dynamic performance of multiply-articulated vehicles [Master's thesis]. Vancouver, Canada: The University of British Columbia; 2001
- [2] Melo RP. Avaliação da estabilidade lateral de CVCs [Master's thesis]. Brazil: Pontifical University Catholic of Parana; 2004
- [3] Ledesma R, Shih S. Heavy and medium duty vehicle suspension-related performance issues and effective analytical model for system design guide. International Truck & Bus Meeting & Exposition. SAE International; 1999. DOI: 10.4271/1999-01-3781
- [4] Rill G. Road Vehicle Dynamics: Fundamentals and Modeling. Boca Ratón, Florida: CRC Press; 2011. ISBN: 978-1-4398-3898-3
- [5] Crossley FRE. A contribution to Grübler's theory in number synthesis of plane mechanisms. ASME Journal of Engineering Industry. 1964;86(2):1-8
- [6] Kutzbach K. Mechanische leitungsverzweigung, ihre gesetze und anwendungen. Maschinenbau Betrieb. 1929;8(8):710-716
- [7] Tsai LW. Mechanism Design: Enumeration of Kinematic Structures According to Function. Boca Ratón, Florida: CRC press; 2001. ISBN: 0849309018
- [8] Jazar RN. Vehicle Dynamics: Theory and Application. New York: Springer; 2014. ISBN: 978-1-4614-8544-5
- [9] Pacejka H. Tire and Vehicle Dynamics. Netherlands: Elsevier Ltd; 2012. ISBN: 9780080970165
- [10] Smith ND. Understanding parameters influencing tire modeling. Formula SAE Platform - Department of Mechanical Engineering - Colorado State University; 2004
- [11] Erthal J. Modelo cinestático para análise de rolagem em veículos [PhD thesis]. Florianópolis, Brazil: Universidade Federal de Santa Catarina; 2010
- [12] Lee U. A study on a method for predicting the vehicle controllability and stability using the screw axis theory [PhD thesis]. Seoul, South Korea: Hanyang University; 2001
- [13] Mejia L, Simas H, Martins D. Force capability maximization of a 3rrr symmetric parallel manipulator by topology optimization. In: 22nd International Congress of Mechanical Engineering (COBEM 2013). Ribeirão Preto, SP, Brazil: ABCM - Associação Brasileira de Engenharia e Ciências Mecânicas; 2013
- [14] Taylor RK, Bashford LL, Schrock MD. Method for measuring vertical tire stiffness. American Society of Agricultural Engineers. 2000;42(6):1415-1419
- [15] Rill G et al. Leaf spring modelling for real time applications. In: 18th IAVSD-Symposium. Atsugi-Japan.: IAVSD-The International Association for Vehicle System Dynamics; 2003
- [16] Moreno G, Frantz JC, Nicolazzi LC, Vieira RS, Martins D. Stiffness and deformation of mechanisms with locally flexible bodies: A general method using expanded passive joints. In: International Symposium on Advances in Robot Kinematics. Cham: Springer; 2018. pp. 285-292
- [17] Dhoshi NP, Ingole NK, Gulhane UD. Analysis and modification of leaf spring of tractor trailer using analytical and finite element method. International Journal of Modern Engineering Research. 2011;1(2):719-722

- [18] Saf-Holland. About Fifth Wheels. Germany: SAF-HOLLAND – Verkehrstechnik GmbH; 2006
- [19] Kurdi O, Rahman RA, Samin PM. Optimization of heavy duty truck chassis design by considering torsional stiffness and mass of the structure. *Applied Mechanics and Materials*. 2014; **554**:459-463
- [20] Winkler C. Rollover of Heavy Commercial Vehicles. SAE RR-004. Warrendale: Society of Automotive Engineers; 2000. p. 74. ISBN: 978-0-7680-0626-1; <http://books.sae.org/rr-004/>
- [21] Kamnik R, Boettiger F, Hunt K. Roll dynamics and lateral load transfer estimation in articulated heavy freight vehicles. In: *Proceedings of the Institution of Mechanical Engineers: Journal Automobile Engineering*. 2003; **217**(11):985-997
- [22] Davies TH. Mechanical networks— I. Passivity and redundancy. *Mechanism and Machine Theory*. 1983;**18**(2):95-101
- [23] Davies TH. Mechanical networks— III. Wrenches on circuit screws. *Mechanism and Machine Theory*. 1983; **18**(2):107-112
- [24] Davies TH. The 1887 committee meets again. Subject: Freedom and constraint. In: *Ball 2000 Conference*. Cambridge, UK: Cambridge University Press, Trinity College; 2000. p. 56
- [25] Moreno GG, Nicolazzi L, Vieira RS, Martins D. Three-dimensional analysis of the rollover risk of heavy vehicles using Davies method. In: *14th World Congress in Mechanical and Machine Science (IFTToMM2015)*, Taipei, Taiwan; 2015. DOI: 10.6567/IFTToMM.14TH.WC.PS4.006
- [26] Moreno G, Barreto RLP, Nicolazzi L, Vieira R, Martins D. Three-dimensional analysis of vehicles stability using graph theory. In: *Graph-Based Modelling in Engineering*. Switzerland: Springer International Publishing; 2016. DOI: 10.1007/978-3-319-39020-8_9. ISBN: 978-3-319-39018-5
- [27] Moreno G, Nicolazzi L, Vieira RS, Martins D. Modeling and analysis of solid axle suspension and its impact on the heavy vehicles stability. In: *Congresso Nacional de Engenharia Mecânica (CONEM2016)*; Fortaleza, Brazil; 2016. DOI: 10.13140/RG.2.2.32141.33766
- [28] Moreno G, Nicolazzi LC, Vieira RDS, Martins D. Suspension and tyres: Stability of heavy vehicles. *International Journal of Heavy Vehicle Systems*. 2017;**24**(4):305-326. DOI: 10.1504/IJHVS.2017.087221
- [29] Tsai LW. *Robot Analysis—The Mechanism of Serial and Parallel Manipulators*. New York: John Wiley & Sons; 1999. ISBN: 0-471-32593-7
- [30] Davies TH. Couplings, coupling network and their graphs. *Mechanism and Machine Theory*. 1995;**30**(7): 1001-1012
- [31] Heyman J. *Basic Structural Theory*. New York: Cambridge University Press; 2008. ISBN 13: 978-0-511-39692-2
- [32] Moreno G, Nicolazzi LC, Vieira RDS, Martins D. Stability of long combination vehicles. *International Journal of Heavy Vehicle Systems*. 2018; **25**(1):113-131. DOI: 10.1504/IJHVS.2018.089897
- [33] Cabral JC. Randon e Wabco Desenvolvem Sistema Eletrônico Anti-Tombamento Para Bitrens—Agência Intelog Notícias. 2008. Available from: <http://www.newslog.com.br> [Accessed: 19 August 2008]
- [34] Lui P, Rakheja S, Ahmed A. Detection of dynamic roll instability of heavy vehicles for open-loop rollover control. In: *1997 International Truck and*

Bus Meeting. SAE Special Publications
1308 - SAE Paper No. 973263;
Cleveland, Ohio; 1997. pp. 105-112

[42] AASHATO. Recommendation for
AASHTO Superelevation Design.
Washington, D.C.: Design Quality
Assurance Bureau, NYSDOT; 2003

[35] Gillespie TD. Fundamentals of
Vehicle Dynamics. Warrendale, PA:
SAE International; 1992. ISBN:
1560911999

[36] Michelin Ltd. Michelin XZA Tire.
Greenville, SC: Michelin North America,
Inc.; 2013

[37] Harwood DW, Torbic DJ,
Richard KR, Glauz WD, Elefteriadou L.
Review of Truck Characteristics as
Factors in Roadway Design.
Transportation Research Board.
Washington DC: National Cooperative
Highway Research Program; 2003.
ISBN: 0-309-08779-1

[38] Ervin RD, Guy Y. The influence of
weights and dimensions on the stability
and control of heavy duty trucks in
Canada. UMTRI - The University of
Michigan Transportation Research
Institute, Final Report UMTRI-86-35/
III; 1986

[39] Walker HK, Pearson JR.
Recommended regulatory principles for
interprovincial heavy vehicle weights
and dimensions. Tech. Rep., CCMTA/
RTAC Vehicle Weights and Dimensions
Study Implementation Committee
Report; 1987

[40] Woodrooffe J, Sweatman P,
Arbor A, Middleton D, James R,
Billing JR. National Cooperative
Highway Research Program—NCHRP.
Report 671. Review of Canadian
Experience with the Regulation of
Large Commercial Motor Vehicles.
Washington, D.C.: National Academy
of Sciences; 2010. ISBN:
978-0-309-15518-2

[41] AASHTO. A Policy on Geometric
Design of Highways and Streets. Tech.
Rep. 4th ed. Washington, D.C.:
AASHTO; 2001. ISBN: 1-56051-156-7